Standoff Tracking of Medical Interventional Devices using Non-Contact Microwave Thermoacoustic Detection

George Alexopoulos, Kevin C. Boyle, Nemat Dolatsha, Hao Nan, Butrus T. Khuri-Yakub, and Amin Arbabian

Department of Electrical Engineering, Stanford University, Stanford, CA, 94305

Abstract — Tracking of medical interventional devices is performed using non-contact microwave-induced thermoacoustic detection. The interventional device is modeled with an exposed tip coaxial probe in an agar phantom and it uses the inherent microwave excitation to generate modulated thermoacoustic signals. The resulting ultrasound signal is detected by custom designed capacitive micromachined ultrasonic transducers (CMUTs) at a standoff and without any contact with the target. The dependency of the specific absorption rate (SAR) profile on the excitation frequency and probe tip length is examined in order to determine optimal operating conditions for resolution and signal level. An excitation frequency of 2.35 GHz is chosen and is amplitude-modulated with a 72 kHz pulse train to match the center frequency of the CMUTs. A two transducer system is employed to achieve cm-scale resolution via 2-dimensional location tracking using a modified trilateration technique.

Index Terms — biomedical imaging, interventional, medical services, target detection, target tracking, ultrasonic transducers.

I. Introduction

Interventional medical devices enable a wide range of minimally-invasive therapeutic procedures using image guidance to diagnose and treat diseases [1]. Procedures such as angiography, needle biopsy, and localized tissue ablation combine the use of flexible catheter probes and medical imaging techniques to reduce patient risk from highly invasive procedures requiring open surgery [1]. In order to accurately steer the flexible probe of these devices through the patient to the target location, a real-time tracking method must be implemented. Interventional Magnetic Resonance Imaging (iMRI) procedures allow for accurate and interactive visualization of the probe tip and target location using traditional MRI technology [2]. However, these solutions are costly and typically bulky, do not offer easy access to the patient, and require specialized MRI-safe equipment.

Recently, thermoacoustic (TA) methods employing excitation of soft biological tissue at microwave frequencies have been proposed for medical imaging [3-6]. Non-contact thermoacoustic detection is based on the application of microwave excitation, which instantaneously and selectively heats the target tissue causing minute expansions and, therefore, a pressure signal that travels out of the body and is captured by an ultrasonic (US) detector [7]. Using this idea, we propose a non-contact, low-cost active tracking system for interventional probes. This approach offers a significant improvement and flexibility in access to the patient. As seen in Fig. 1, without significant modification to typical interventional ablation probes, we excite the tissue with microwave signals through the probe tip. An array of CMUTs outside the body can locate the probe through accurate trilateration of the ultrasonic signal generated at the exposed tip via the thermoacoustic effect [8]. Here, the patient is not confined to a typical bulky scanner used in iMRI and the CMUT receiver array can be relocated around the target. It should be noted that the non-contact operation introduces a large 65-dB acoustic signal loss at the air-body interface and to recover the SNR the system requires sensitive ultrasound detectors, typically capacitive (or piezoelectric) micromachined ultrasonic transducers (CMUTs) [9-11]. Though this initial proof of concept system uses a low-bandwidth transducer array that only allows for cm-scale resolution, we project that a more wideband US receive system utilizing more CMUT array elements would allow resolution down to the mm-scale. We have verified the concept of this technique through full-wave electromagnetic simulations as well as experiments.

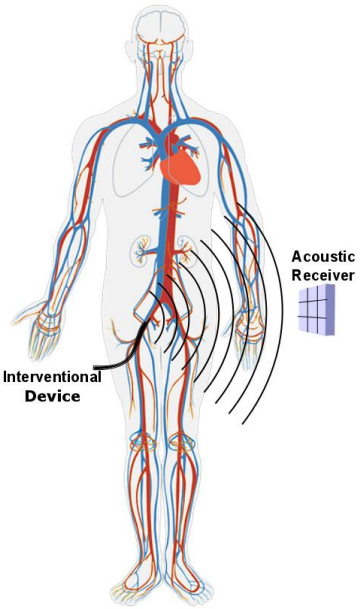

Fig. 1. Conceptual schematic of system for tracking interventional probes through thermoacoustic detection.

978-1-5090-0698-4/16/$31.00 ©2016 IEEE

II. Simulations

Typical interventional devices such as catheter probes or ablation probes consist of an insulating shaft followed by an exposed tip that deposits microwave energy according to the needs of the medical procedure. The tip can be modeled by a typical coaxial cable with its inner conductor partially exposed to the medium. Biological tissue is modeled using an Agarose solution gel which acts as the tissue phantom for the acoustic and electric properties [12]. Microwave energy radiates from the coaxial probe and is absorbed by the tissue immediately surrounding the exposed tip area. In this approach, the microwave frequency and the length of the exposed inner conductor tip are important factors in the deposition of microwave power into tissue.

The exposed tip acts in a similar manner to a monopole antenna when driven with microwave excitation. In order to have a higher resolution in detecting the position of the tip, it is important for the deposited microwave energy to be absorbed within a small volume around the exposed tip. This can be addressed by i) operating at higher microwave frequencies where the microwave attenuation rate in tissue is high, or by ii) choosing a very small length (compared to the wavelength in the medium) for the exposed area of the tip. Microwave absorption in tissue increases with frequency and is relatively high at GHz frequencies [4]. As a compromise between microwave absorption properties and the complexity of designing an efficient and scalable probe system, we have chosen the frequencies of 1 GHz and 2.35 GHz to investigate further.

Figure 2 shows the simulated SAR distribution around the tip when exposed to the tissue (modeled by agar gel with measured ε_r=70, tanδ=0.257, and mass density of 1.032 g/cm^3 at 2.35 GHz). We have performed simulations for two different frequencies (1, 2.35 GHz) and different tip lengths (λ/10, λ/8, λ/6, λ/4). Table I shows the input impedance of the coaxial probe at the beginning of the tip and the local total SAR in a cylindrical volume with a diameter of 10 mm around the exposed tip for different lengths of the tip. The value of the SAR is normalized to an input microwave peak power of 4kW (13.8 W average) when the input port is assumed matched. The covered section of the 50 Ω coaxial probe is also assumed to be lossless in simulations.

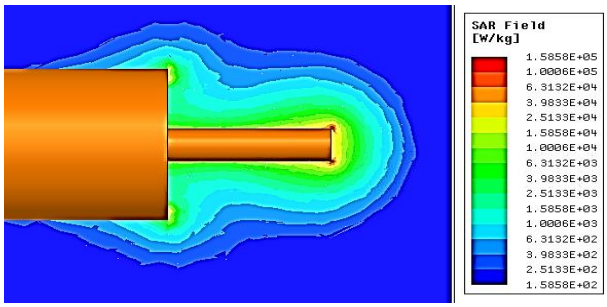

Fig. 2. Simulation of local SAR field magnitudes in log scale around exposed probe tip. Input power is 1 W and the probe is not matched to the source.

TABLE I
Exposed Tip Input Impedance and Power Absorbed By Tissue Under Ideal Matching

Tip Length (λ= λeff)	ZIN (Ω)		Pabs (W/kg)	
	1 GHz	2.35 GHz	1 GHz	2.35 GHz
λ/4	12.18-j*4.71	7.82-j*1.00	0.863	1.07
λ/6	8.96-j*9.57	5.76-j*5.23	0.984	1.15
λ/8	8.25-j*13.29	5.45-j*8.15	1.17	1.27
λ/10	8.15-j*16.34	5.50-j*10.41	1.28	1.37

As explained earlier, the total SAR in a confined volume around the tip is slightly higher at 2.35 GHz compared to 1 GHz. Moreover, smaller tip lengths show more localized power absorption. However, due to the ease of fabrication and impedance matching we have chosen the λ/4 case at 2.35 GHz (L=3.81mm) in our experimental setup.

III. Experiment Setup

Figure 3 shows the experimental setup. The probe tip was made by cutting an RG-58U coaxial cable and exposing the appropriate length of inner conductor. A solution of UltraPure Agarose (Invitrogen) and sodium chloride was prepared and allowed to set into a gel. The probe input was matched to the microwave source using a triple-stub tuner and a VNA. The function generator was used to create a modulation signal of N=10 pulses in a burst with a 20 ms burst period at a pulse frequency of 72 kHz, which matches the center frequency of the two CMUT detectors. The wavelength of the ultrasound signal in agar is 2.14 cm at this frequency. For coherent processing, this pulse was synchronized to the oscilloscope to determine the onset time of the signal to the sample. The pulse train then modulated the microwave excitation at a carrier frequency of 2.35 GHz. The modulated pulse signal was then amplified to a peak of 4 kW and the resulting signal was applied to the probe tip. The generated US signals were detected by highly-sensitive CMUTs, amplified through an LNA, and shown on the oscilloscope. Averaging was performed with N_{avg} = 100.

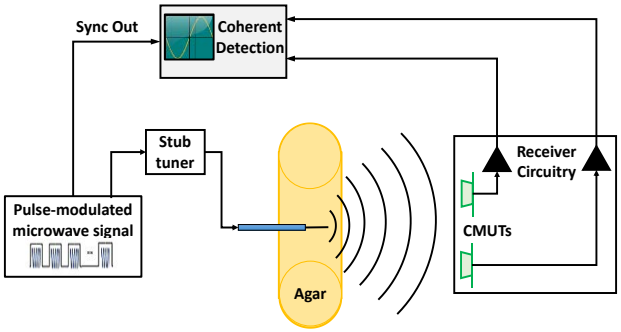

Fig. 3. Schematic representation of the experiment setup.

IV. Results and Discussion

The experiment was designed to use trilateration techniques to measure the position of the tip in the plane of the US setup using two transducers. This creates two solution points where one is located vertically above the transducers and is therefore ignored. The other solution gives the vertical distance below and the horizontal distance away from the CMUTs. The actual vertical distance between the surface of the agar gel and CMUTs remained constant at 40 cm. The agar gel was molded into the shape of a long cylinder and placed in parallel with the CMUT axis. The probe tip was inserted in 5 cm increments along this axis, at the approximate locations of -10, -5, 0, and 5 cm, where the 0 cm point represented the midpoint of the two CMUTs. The measurement at -10 cm was included to show performance at the edge of the CMUTs' field of view.

The signal time-of-flight was measured from the oscilloscope (example for the 0 cm case shown in Fig. 4) using the time difference between the onset of the excitation microwave pulse train to the left and the onset of the US signal at the CMUTs (shown with markers). A thresholding scheme was employed to identify the signal arrival time at each CMUT. From this and the known vertical distance from the CMUTs to the agar surface, two curves were created, corresponding to possible probe tip location measurements for each CMUT. Refraction due to different acoustic wave velocities in air and agar was accounted for in these curves [13-14]. It is noted that the effective wavelength for 72 kHz ultrasound is 2.14 cm in agar and 0.48 cm in air. The intersection of the two curves gave the actual measured location. For clarity, the setup along with one location calculation for the x-direction 0 cm case is shown in Fig. 5.

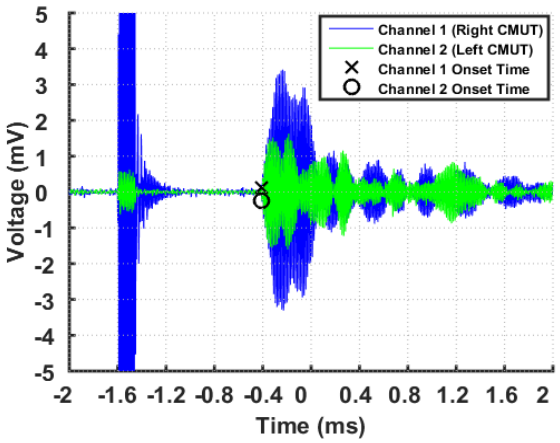

Fig. 4. Waveform showing onset of US signal used in time-of-flight calculations. Signal resulting from multipath reflection is seen after the initial onset of US signal.

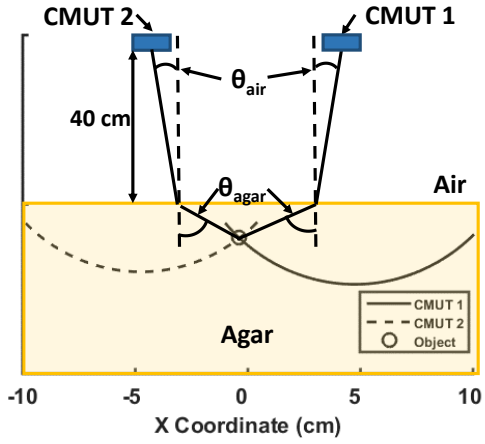

Fig. 5. Calculation of probe tip location with refraction.

TABLE II
Standard Deviation of Measurement Location at Each Probe Tip Position for N = 100, 500, and 1000 Averages

Probe Tip Location (cm)	Standard Deviation of Measurement Location, σ (cm)		
	N_{avg} = 100	N_{avg} = 500	N_{avg} = 1000
5 cm	0.92	0.65	0.29
0 cm	0.52	0.35	0.28
-5 cm	0.64	0.51	0.35
-10 cm	1.21	0.81	0.74

For each probe position, 100 measurements were taken to determine the standard deviation of the position estimate. Position estimates were not compared to the exact 5 cm increments due to the approximate nature of the probe placement. Figure 6 shows a box and whisker plot for the measured position at each approximate position in the horizontal dimension for N_{avg}=100. Table II shows the standard deviation of the measurement location for N_{avg}=100, N_{avg}=500, and N_{avg}=1000. Averages of 500 and 1000 were applied by averaging groups of five and ten measurements respectively from the original N_{avg}=100 dataset. In order to maintain a constant sample size for standard deviation calculations 10

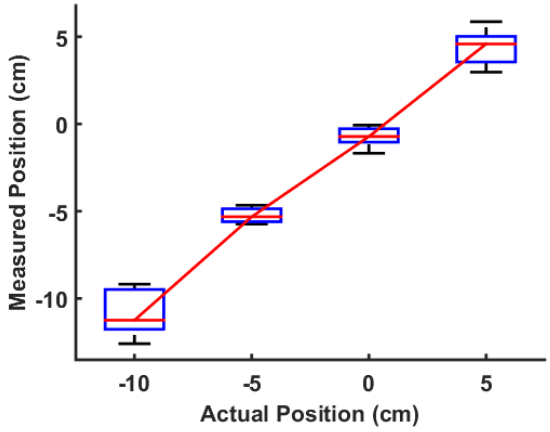

Fig. 6. Box and whisker plot for measured position vs. actual position in the horizontal dimension with *N=100* averages.

position measurements were selected from the N_{avg}=100 and N_{avg}=500 datasets corresponding to the maximum sample size of the N_{avg}=1000 dataset.

With averaging, assuming additive white Gaussian noise, and using the Cramer-Rao lower bound (CRLB) for pulse arrival time variance, the error in the measured location is expected to improve [15]. This was confirmed by the results in Table II by the reduction of the standard deviation with averaging across all probe tip locations. We see that for probe positions outside of the aperture of the CMUTs, the measured position experienced increased deviation from the location estimate. This indicates the probe tip is leaving the aperture of the tracking system thus decreasing the signal levels measured by the CMUTs and this increases the pulse arrival time uncertainty. Further improvements to the location estimate may be achieved with more sophisticated threshold detection algorithms and coherent processing techniques to increase SNR and bandwidth. Precise comparison of estimated and actual position may be evaluated with a carefully designed experimental setup.

V. Conclusion

We propose and experimentally demonstrate a non-contact tracking system for medical interventional devices such as catheter probes or ablation probes. Our system presents a modulation on the microwave excitation that is already present in the device, to generate coherent US signatures from the volume immediately surrounding tissue via the TA effect. These US signals are then detected using CMUTs in a trilateration scheme. Interventional devices and human tissue are modeled with exposed tip coaxial probes in an agar phantom. Measurements of probe tip location using two CMUTs indicate accurate tracking at cm-scale resolution over a range of locations within the aperture of the tracking array and increasing error for locations outside the aperture. The proposed standoff tracking method avoids the fixed device structure setups present in typical iMRI procedures and allows for freedom of movement and placement of both the tracking setup and the patient under examination. Future work includes reducing location tracking error by developing more advanced signal detection algorithms and improving the accuracy of the trilateration scheme by employing a more mobile, wideband, and multi-element US receive array.

Acknowledgements

The authors acknowledge Rohde & Schwarz for measurement equipment as well as ANSYS for the HFSS simulation software. This work was supported in part by the DARPA MEDS program and the Stanford CIS seed grant. Special thanks to Dr. Greig Scott for valuable comments and suggestions.

References

[1] H. Song, *et al.,* "Development of a needle insertion end-effector for interventional radiology," *Int. Symp. On Robotics.*, Seoul, Oct. 2013, pp.*1-3*.

[2] G. Scott *et al.*, "Electro/magneto/thermal acoustic ultrasound generation in iMRI devices," in *Interventional MRI Symp.*, Leipzig, 2014.

[3] R. A. Kruger *et al.*, "Thermoacoustic computed tomography of the breast at 434 MHz," *Int. Microwave Symp.*, Anaheim, CA, June 1999, pp. *591-594*.

[4] L. V. Wang, "Microwave induced acoustic (thermoacoustic) tomography," in *Photoacoustic Imaging and Spectroscopy*, Boca Raton: CRC Press, 2009, ch. 27, pp. *339-340*.

[5] H. Nan and A. Arbabian, "Stepped-Frequency Continuous-Wave Microwave-Induced Thermoacoustic Imaging," *Appl. Phys. Lett.*, vol. 104, pp. 224104, 2014.

[6] H. Nan, T. Chou, and A. Arbabian, "Segmentation and Artifact Removal in Microwave-Induced Thermoacoustic Imaging", *Eng. in Medicine and Biology Society (EMBC)*, pp.4747,4750, 26-30 Aug. 2014.

[7] H. Nan *et al.*, "Non-contact thermoacoustic detection of embedded targets using airborne-CMUTs," *Appl. Phys. Lett.*, vol. 106, no. 8, 084101, Feb., 2015.

[8] R. Misra, S. Shukla, and V. Chandel, "Lightweight localization using trilateration for sensor networks," *Int. J. Wireless Inf. Networks*, vol. 21, no. 2, pp. 89-100, May 2014.

[9] A. Nikoozadeh and P. T. Khuri-Yakub, "CMUT with substrate-embedded springs for non-flexural plate movement," *Int. Ultrasonics Symp.*, San Diego, CA, Oct. 2010, pp. *1510-1513*.

[10] A. Nikoozadeh *et al.*, "Forward-looking intracardiac imaging catheters using fully integrated CMUT arrays," *Int. Ultrasonics Symp.*, San Diego, CA, Oct. 2010, pp. *770-773*.

[11] D. E. Dausch *et al.*, "In vivo real-time 3-D intracardiac echo using PMUT arrays," *IEEE Transactions on Ultrasonics, Ferroelectrics, and Frequency Control*, vol. 61, no. 10, Oct. 2014.

[12] J. E. Browne, K. V. Ramnarine, A. J. Watson, and P. R. Hoskins, "Assessment of the Acoustic Properties of common tissue-mimicking test objects," *Ultrasound in Medicine & Biology,* vol. 29, pp. 1053-1060, 2003.

[13] H. Shin *et al.*, "Estimation of average speed of sound using deconvolution detection of medical ultrasound data," Ultrasound in Med. & Biol. 36, no. 4, pp. 623-636, Jan. 2010.

[14] P. Filippi *et al.*, "Outdoor sound propagation," in *Acoustics: Basic Physics, Theory, and Methods*, 1st ed. London, UK: Academic Press, 1999, ch. 4, sec. 4.3.2, pp. 150-151.

[15] H. L. Van Trees, *Detection, Estimation, and Modulation Theory, Radar-Sonar Signal Processing and Gaussian Signal in Noise.* Wiley-Interscience, May 2003.